AIP | Applied Physics Letters

Detection of Cu2Zn5SnSe8 and Cu2Zn6SnSe9 phases in co-evaporated Cu2ZnSnSe4 thin-films

Torsten Schwarz, Miguel A. L. Marques, Silvana Botti, Marina Mousel, Alex Redinger, Susanne Siebentritt, Oana Cojocaru-Mirédin, Dierk Raabe, and Pyuck-Pa Choi

Citation: Applied Physics Letters **107**, 172102 (2015); doi: 10.1063/1.4934847
View online: http://dx.doi.org/10.1063/1.4934847
View Table of Contents: http://scitation.aip.org/content/aip/journal/apl/107/17?ver=pdfcov
Published by the AIP Publishing

Detection of $Cu_2Zn_5SnSe_8$ and $Cu_2Zn_6SnSe_9$ phases in co-evaporated $Cu_2ZnSnSe_4$ thin-films

Torsten Schwarz,[1,a),b)] Miguel A. L. Marques,[2] Silvana Botti,[2,c)] Marina Mousel,[3] Alex Redinger,[3,d)] Susanne Siebentritt,[3] Oana Cojocaru-Mirédin,[1,a)] Dierk Raabe,[1] and Pyuck-Pa Choi[1,e)]

[1]*Max-Planck-Institut für Eisenforschung GmbH, Max-Planck-Straße 1, 40237 Düsseldorf, Germany*
[2]*Institut Lumière Matière (UMR5306) and ETSF, Univerité Lyon 1-CRNS, Université de Lyon, F-69622 Villeurbanne, France*
[3]*Laboratory for Photovoltaics, University of Luxembourg, 41, rue du Brill, L-4422 Belvaux, Luxembourg*

(Received 17 July 2015; accepted 18 October 2015; published online 28 October 2015)

$Cu_2ZnSnSe_4$ thin-films for photovoltaic applications are investigated using combined atom probe tomography and *ab initio* density functional theory. The atom probe studies reveal nano-sized grains of $Cu_2Zn_5SnSe_8$ and $Cu_2Zn_6SnSe_9$ composition, which cannot be assigned to any known phase reported in the literature. Both phases are considered to be metastable, as density functional theory calculations yield positive energy differences with respect to the decomposition into $Cu_2ZnSnSe_4$ and ZnSe. Among the conceivable crystal structures for both phases, a distorted zinc-blende structure shows the lowest energy, which is a few tens of meV below the energy of a wurtzite structure. A band gap of 1.1 eV is calculated for both the $Cu_2Zn_5SnSe_8$ and $Cu_2Zn_6SnSe_9$ phases. Possible effects of these phases on solar cell performance are discussed. © *2015 AIP Publishing LLC*. [http://dx.doi.org/10.1063/1.4934847]

Kesterite structured compound semiconductors $Cu_2ZnSn(S,Se)_4$ (CZTSSe) are of rapidly growing interest as materials for photovoltaic applications.[1–4] These compounds exhibit high absorption coefficients as well as direct energy band gaps (~1–1.5 eV) and comprise low cost, non-toxic, and earth abundant elements.[1] Thus, CZTSSe films are considered as highly promising absorbers for thin-film solar cells.

The current record energy conversion efficiency of CZTSSe-based solar cells is 12.6%,[2] which is still far below that of chalcopyrite compounds $Cu(In,Ga)(S,Se)_2$ (21.7%).[5] One of the main reasons for the limited performance of CZTSSe solar cells is the difficulty to prepare single phase CZTSSe without the formation of secondary phases. Both theoretical and experimental data show that CZTSSe compounds have a very narrow existence region, with only 1%–2% absolute deviation from nominal stoichiometry.[6–9] Moreover, evaporation of volatile S(e) and SnS(e)[10–12] and the presence of a reactive Mo back contact can cause the decomposition of CZTSSe into secondary phases.[13]

Several secondary phases have been reported for CZTSSe thin-films such as ZnS(e),[14–17] $Cu_xS(e)$,[18,19] $Cu_2SnS(e)_3$,[20,21] and $SnS(e)_x$.[15,18] Secondary phases are generally considered to be detrimental to cell efficiency, as they increase the recombination rates and consequently cause a loss in open-circuit voltage and/or can lead to an increase in series resistance.[4,14] Hence, reliable and accurate characterization of the secondary phase precipitates with respect to their composition, size, and spatial distribution within the absorber is essential for understanding the solar cell properties and controlling the synthesis and process parameters. Detection of secondary phases remains a great challenge, as many of them are structurally similar to the CZTSSe matrix and are formed as nanosized precipitates.

Recently, we reported on the detection of a complex network of nanometer-sized ZnSe grains within a CZTSe absorber layer[22] using atom probe tomography (APT).[23] The absorber had been prepared by the low-temperature co-evaporation of a precursor (320 °C substrate temperature), followed by etching in a KCN-solution and post-deposition annealing at 500 °C. APT analyses of this absorber also revealed that some of the detected ZnSe grains contained Cu- and Sn-rich precipitates, which could not be attributed to any known equilibrium phase.[17] However, it was not possible to clearly understand the complex atomic-scale processes occurring during absorber fabrication.

For gaining better understanding of the characteristics of final absorbers, we focus on initial precursor films in this work. We note that the elemental diffusion during precursor growth is limited due to the low substrate temperature (320 °C). It has been reported for various materials that low fabrication/processing temperatures suppress the formation of equilibrium compounds due to limited diffusion kinetics.[24,25] Instead, metastable phases can be formed,[24,25] which can significantly affect the electrical and/or optical properties of a device. Thus, the low-temperature growth of compound semiconductors can be a viable means of studying intermediate phases with versatile properties.

Here, we report on the discovery of two metastable phases of $Cu_2Zn_5SnSe_8$ and $Cu_2Zn_6SnSe_9$ composition, which have not been observed in CZTSe films before. *Ab initio* density functional theory (DFT) calculations have been carried

[a)]Present address: I. Physikalisches Institut IA, RWTH Aachen University, 52056 Aachen, Germany.
[b)]Electronic mail: schwarz@mpie.de
[c)]Present address: Institute of Condensed Matter Theory and Solid State Optics, Friedrich-Schiller University Jena, Max-Wien-Platz 1, 07743 Jena, Germany.
[d)]Present address: Helmholtz-Zentrum Berlin, Department Complex Compound Semiconductor Materials for Photovoltaics, Hahn-Meitner-Platz 1, 14109 Berlin, Germany.
[e)]Electronic mail: choi@mpie.de

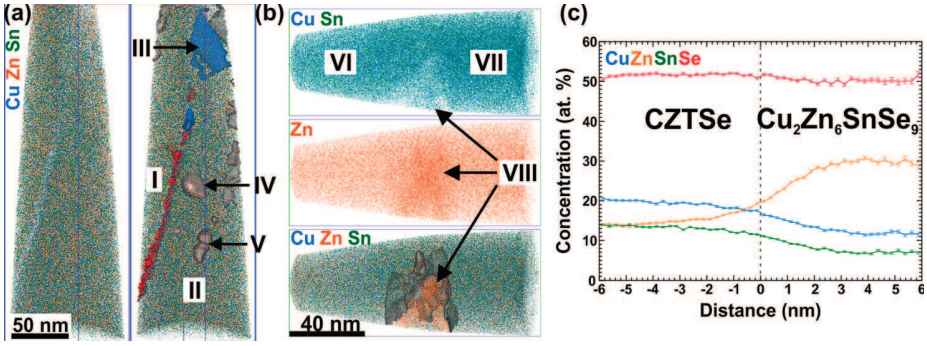

FIG. 1. (a) and (b) Three-dimensional elemental maps of Cu (blue), Zn (orange), and Sn (green) with iso-concentration surfaces of 20.0 at. % Zn (grey), 22.5 at. % Cu (red), and 25.0 at. % Cu (blue). (c) Proximity histogram (proxigram) across the 20.0 at. % Zn iso-concentration surface of region VIII. Reprinted with permission from T. Schwarz, "On the nano-scale characterization of kesterite thin-films." Ph.D. dissertation (RWTH Aachen, 2015).[50]

out in order to assess the stability of these phases and to validate the experimental observations. Based on the band gap calculations, we also discuss the possible effects of the discovered phases on solar cell performance.

Two different CZTSe precursor films were grown in a molecular beam epitaxy system by co-evaporation of Cu, Zn, Sn, and Se onto a Mo-coated soda-lime glass substrate at 320 °C.[22] To fabricate the solar cell absorbers, these films are typically annealed afterwards at elevated temperatures. The first sample was grown under Cu-rich [Cu]/([Zn] + [Sn]) > 1 and Zn-rich [Zn]/[Sn] > 1 conditions, while the second sample was grown under Cu-poor [Cu]/([Zn] + [Sn]) < 1 and Zn-rich [Zn]/[Sn] > 1 conditions.

The preparation of APT samples was carried out using a dual-beam focused-ion-beam (FIB) (FEI Helios Nanolab 600i). In order to reduce the Ga implantation to a negligible level, a low energy (5 keV) Ga beam was used for final shaping of the APT tips.

APT analyses were performed using a local electrode atom probe (LEAP^{TM} 3000X HR, Cameca Instruments). Laser pulses of 532 nm wavelength, 12 ps pulse length, and an energy of 50 pJ were applied at a temperature of 50 K. DFT calculations were performed to validate the APT data and find a stable structure related to the composition detected by APT.

Figs. 1(a) and 1(b) show 3D elemental maps pointing towards the surface of two different regions from the same Cu-rich film. While the first dataset stems from a region less than 200 nm below the surface, the second one is from a region less than 500 nm above the Mo back contact (film thickness is about 2 μm). For clarity, only Cu (blue), Zn (orange), and Sn (green) atoms are shown on the left in Fig. 1(a). In addition, iso-concentration surfaces of 20.0 at. % Zn (grey), 22.5 at. % Cu (red), and 25.0 at. % Cu (blue) highlight compositional variations, as shown on the right in Fig. 1(a). The Zn iso-concentration surface marks the Zn-rich regions, which are Cu and Sn depleted. The 22.5 at. % Cu iso-concentration surface shown in red marks a planar Cu-enriched and Sn-depleted zone which corresponds most probably to a grain boundary. The blue Cu iso-concentration surface (25.0 at. %) marks Cu-rich precipitates, formed at the grain boundary. Table I lists the compositions of the regions in Figs. 1(a) and 1(b), labelled as I-VIII. The values were determined from mass spectrum analyses, applying a peak deconvolution algorithm to overlapping mass peaks (included in the software IVAS 3.6.6, Cameca Instruments). The errors given in Table I are 2σ standard deviations, which result from the limited sampling volumes. A series of APT measurements with varying temperature and laser pulse energy showed that the composition of the CZTSe phase remains nearly constant. Therefore, we may conclude that systematic errors due to the excessive heating of the specimen during laser pulsing and preferential field evaporation of selective species do not play a significant role.

We observe Cu-poor ([Cu]/([Zn] + [Sn]) < 1) CZTSe regions (I-II and VI-VII), being almost stoichiometric in [Zn]/[Sn], although the overall composition of the film is Cu-rich ([Cu]/([Zn] + [Sn]) > 1) and Zn-rich ([Zn]/[Sn] > 1). Region III in Fig. 1(a) is identified as $Cu_{2-x}Se$ with a small

TABLE I. Chemical composition measured by APT from different regions of the corresponding precursor layer. Regions I-VIII are shown in Fig. 1. Regions IX–XI refer to other datasets (not shown here) from both Cu-rich and Cu-poor precursors. Regions IV, V, and VIII-XI highlighted in bold are $Cu_2Zn_5SnSe_8$ and $Cu_2Zn_6SnSe_9$. Due to the high standard deviation of the compositions of regions V, IX, and X, a clear phase assignment of these regions to either $Cu_2Zn_5SnSe_8$ or $Cu_2Zn_6SnSe_9$ is not feasible. Reprinted with permission from T. Schwarz, "On the nano-scale characterization of kesterite thin-films." Ph.D. dissertation (RWTH Aachen, 2015).[50]

Region	Cu (at. %)	Zn (at. %)	Sn (at. %)	Se (at. %)	[Cu]/([Zn] + [Sn])	[Zn]/[Sn]
I	18.9 ± 0.1	14.1 ± 0.1	14.3 ± 0.1	52.5 ± 0.2	0.67	0.98
II	20.9 ± 0.1	13.7 ± 0.1	14.2 ± 0.1	51.2 ± 0.1	0.75	0.96
III	52.6 ± 1.2	2.0 ± 0.4	1.8 ± 0.3	43.6 ± 1.2	13.80	1.16
IV	9.4 ± 0.5	34.4 ± 0.8	5.6 ± 0.4	50.6 ± 0.9	0.23	6.12
V	11.2 ± 0.9	32.4 ± 1.4	6.5 ± 0.7	50.0 ± 1.5	0.29	4.96
VI	21.1 ± 0.2	13.9 ± 0.2	12.6 ± 0.2	52.4 ± 0.2	0.80	1.10
VII	21.4 ± 0.3	12.8 ± 0.2	14.3 ± 0.2	51.4 ± 0.3	0.79	0.90
VIII	10.9 ± 0.1	32.9 ± 0.2	5.5 ± 0.1	50.7 ± 0.2	0.28	5.95
IX	11.8 ± 1.0	31.9 ± 1.5	6.2 ± 0.8	50.1 ± 1.6	0.31	5.10
X	11.9 ± 1.0	33.9 ± 1.5	5.5 ± 0.7	48.7 ± 1.6	0.30	6.18
XI	12.3 ± 0.3	31.3 ± 0.4	6.4 ± 0.2	49.9 ± 0.5	0.33	4.86

amount of Zn (2.0 ± 0.4 at. %) and Sn (1.8 ± 0.3 at. %). $Cu_{2-x}Se$ as well as ZnSe precipitates (not shown here) were repeatedly detected in the Cu-rich precursor by APT. Hence, the excess Cu and Zn atoms provided by the Cu- and Zn-rich conditions partition into $Cu_{2-x}Se$ and ZnSe, respectively, according to the phase diagram by Dudchak *et al.*[8] In the Cu-poor precursor, we do not detect $Cu_{2-x}Se$ due to a lack of excess Cu but a small amount of ZnSe.

In addition to $Cu_{2-x}Se$ and ZnSe, two other phases are detected in the Cu-rich precursor by APT. Regions IV and V in Fig. 1(a) and region VIII in Fig. 1(b) (another APT dataset) show compositions significantly deviating from the ZnSe stoichiometry. The compositions of these regions correspond to $Cu_2Zn_5SnSe_8$ and $Cu_2Zn_6SnSe_9$, respectively. A typical proximity histogram across the interface between $Cu_2Zn_6SnSe_9$ and the matrix is shown in Fig. 1(c). We performed several measurements on the identical Cu-rich precursor sample and detected regions of $Cu_2Zn_5SnSe_8$ and $Cu_2Zn_6SnSe_9$ composition several times (listed in Table I). We observed the $Cu_2Zn_5SnSe_8$ phase in a Cu-poor and Zn-rich precursor (co-evaporated at 320 °C) as well (XI in Table I). We did not detect the $Cu_2Zn_6SnSe_9$ phase in the Cu-poor precursor, but its presence cannot be excluded due to the small volumes probed by APT and limited number of measurements. The X-ray diffraction (XRD) pattern of the Cu-rich precursor shows only reflections from $Cu_2ZnSnSe_4$ and $Cu_{1.82}Se$.[22] This observation indicates that $Cu_2Zn_5SnSe_8$ and $Cu_2Zn_6SnSe_9$ have similar structures as $Cu_2ZnSnSe_4$ and ZnSe and/or both phases have a small volume fraction. Raman measurements using an Ar-ion laser (514.5 nm) were also performed, but they showed no additional modes to those, which could be assigned to the matrix. The reasons for this observation are likely the same as for XRD. Indeed, Berg *et al.*[26] showed that, e.g., ZnS, having a similar structure as Cu_2ZnSnS_4, is qualitatively not discernable by Raman (green-wavelength excitation) and also not by XRD if the volume fraction of ZnS is $<10\%$.

The formation of $Cu_2Zn_5SnSe_8$ and $Cu_2Zn_6SnSe_9$ may be due to the Zn-rich growth conditions and the limited diffusivity of Zn at low temperatures,[10] which in turn impedes the formation of only CZTSe and ZnSe.

At this point, the question arises whether the regions of $Cu_2Zn_5SnSe_8$ and $Cu_2Zn_6SnSe_9$ compositions can indeed be regarded as energetically stable. Synthesis of these phases by high-temperature solid state reaction at 750 °C failed, indicating that both phases are metastable.

DFT calculations were performed to examine whether there is an energetically stable structure for the experimental compositions. Calculations were performed using the all-electron projector augmented wave method as implemented in the code vasp.[27,28] We used a plane-wave cutoff of 520 eV and a number of k-points in direction α given by about $|b_\alpha|/(0.022 \times 2\pi)$, where b is the reciprocal lattice vector. The minima hopping algorithm for global structural prediction indicated that distorted zinc-blende phases are the low-energy structures for supercells with the stoichiometry of $Cu_2Zn_5SnSe_8$ and $Cu_2Zn_6SnSe_9$, as measured by APT.[29,30] Therefore, we built supercells consisting of 48 and 54 atoms with the stoichiometry of $Cu_2Zn_5SnSe_8$ and $Cu_2Zn_6SnSe_9$ starting from zinc-blende and wurtzite units and allowed for random exchange of Cu, Zn, and Sn atoms on the cation sublattice sites, using a procedure that resembles the outer loop of the minima hopping method.[30]

These further optimization steps were performed within DFT using a PBE + U exchange correlation functional (with $U = 5$ eV on Cu d states).[31] The lowest-energy structures were all optimized by ensuring numerical convergence to less than 2 meV/atom. Many similar zinc-blend-like structures that differ by less than 20 meV (i.e., by less than k_BT at room temperature $T = 300$ K, k_B—Boltzmann constant) per atom can be obtained by exchanging the type of atom at certain cation lattice sites. Moreover, the lowest-energy structures obtained starting from wurtzite units are higher in energy by only few tens of meV. This proves that the configuration disorder plays a relevant role in these compounds and that different phases are likely to coexist in experimental samples. Keeping this fact in mind, we show in Fig. 2 the lowest energy structure of $Cu_2Zn_5SnSe_8$ and $Cu_2Zn_6SnSe_9$ compatible with the size of our supercells, where zinc-blende Zn sites are occupied by Zn (grey), Cu (blue), or Sn (rose). The lattice parameters of the 16 and 36 atom unit cells are $a = 30.9$ Å, $b = 5.7$ Å, $c = 20.7$ Å, $\alpha = 90°$, $\beta = 168°$, and $\gamma = 90°$ for $Cu_2Zn_5SnSe_8$ and $a = 8.1$ Å, $b = 10.8$ Å, $c = 10.8$ Å, $\alpha = 69°$, $\beta = 79°$, and $\gamma = 79°$ for $Cu_2Zn_6SnSe_9$, respectively. See the supplementary material in Ref. 32 for the crystallographic information files. The presence of three different cations on zinc-blende Zn sites induces the distortion of the original cubic symmetry. Furthermore, the Cu atoms build up a ladder like structure.

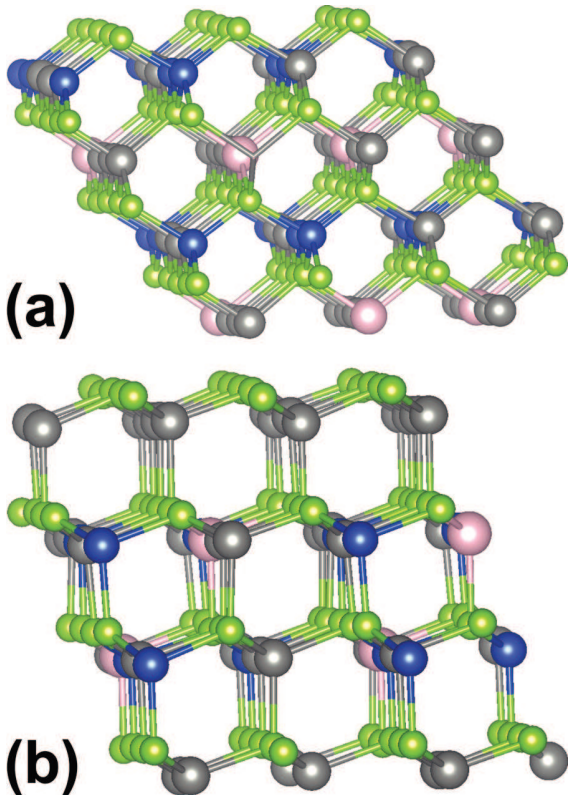

FIG. 2. Distorted colored zinc-blende structure of (a) the $Cu_2Zn_5SnSe_8$ and (b) $Cu_2Zn_6SnSe_9$ phase calculated by DFT: Cu (blue), Zn (grey), Sn (rose), and Se (green). Reprinted with permission from T. Schwarz, "On the nanoscale characterization of kesterite thin-films." Ph.D. dissertation (RWTH Aachen, 2015).[50]

The Heyd-Scueseria-Ernzerhof (HSE06) hybrid functional was used to calculate the band gap and the density of states (DOS),[33] as this functional proved to be particularly accurate for CZTSe.[34] In Fig. 3, we show the calculated DOS of $Cu_2Zn_5SnSe_8$ and $Cu_2Zn_6SnSe_9$ together with the DOS of kesterite structured $Cu_2ZnSnSe_4$, obtained from the HSE06 Kohn-Sham band structures. We used the tetrahedron method to integrate over the Brillouin zone, with grids of $8 \times 8 \times 8$, $4 \times 6 \times 6$, and $4 \times 4 \times 6$ k-points for $Cu_2ZnSnSe_4$, $Cu_2Zn_5SnSe_8$, and $Cu_2Zn_6SnSe_9$, respectively. The direct band gap for both $Cu_2Zn_5SnSe_8$ and $Cu_2Zn_6SnSe_9$ was calculated to be 1.1 eV, in comparison to the value of 1.0 eV obtained within the same approximation for the kesterite structure of $Cu_2ZnSnSe_4$.[34] One might expect a large increase in the band gap due to alloying between $Cu_2ZnSnSe_4$ and ZnSe, where ZnSe has a larger band gap with 2.82 eV.[35] However, due to the negligible effect of Zn states on the conduction band minimum and valence band maximum of Cu-Zn-Sn-Se compounds,[36] the band gaps are very similar. We can estimate the band offset between different phases by aligning their branch point energies.[37] As a result, there is no offset between $Cu_2ZnSnSe_4$ and $Cu_2Zn_5SnSe_8$ or $Cu_2Zn_6SnSe_9$, respectively, for the conduction band minima. This implies the alignment of the top valence of $Cu_2Zn_5SnSe_8$ and $Cu_2Zn_6SnSe_9$ and a small offset of 0.1 eV between the kesterite phase and these two phases. However, the dispersion and the width of the first narrow conduction band, which is separated from the higher conduction states by a second energy gap,[38] is significantly different for $Cu_2Zn_5SnSe_8$. Besides $Cu_2Zn_5SnSe_8$ and $Cu_2Zn_6SnSe_9$, other compounds being iso-electronic with ZnSe can exist. Therefore, starting from $Cu_2ZnSnSe_4$, a ZnSe pair was added step by step maintaining the octet rule, and the thermodynamic stability with respect to the decomposition into binaries (CuSe, Cu_2Se, ZnSe, SnSe, $SnSe_2$), into the ternary compound Cu_2SnSe_3, and into $Cu_2ZnSnSe_4 + ZnSe$ was calculated. Table II shows a summary of the calculated energy difference of each compound with respect to the energetically favored decomposition paths. In Table II, CuSe and SnSe present the lowest-energy binaries among other Cu_xSe_y and Sn_xSe_y compounds. According to our calculations, $Cu_2Zn_5SnSe_8$ and $Cu_2Zn_6SnSe_9$ are stable with respect to the decomposition into the binary and ternary compounds, as indicated by the negative energy differences (see Table II). The most favorable decomposition is always the one into CZTSe + nZnSe, where *n* is a natural number. Together with $Cu_2Zn_5SnSe_8$, $Cu_2Zn_6SnSe_9$ is the most stable ground state with respect to the decomposition into $Cu_2ZnSnSe_4 + ZnSe$. However, in the final absorbers (post-deposition annealed precursors at 500 °C), we cannot detect these phases. The calculated energy differences with respect to the decomposition into $Cu_2ZnSnSe_4 + ZnSe$ (see Table II) is positive and hence indicate that $Cu_2Zn_5SnSe_8$ and $Cu_2Zn_6SnSe_9$ are metastable phases. Since we do not detect Cu_xSe_y or Sn_xSe_y compounds in the annealed precursors,[17,22] $Cu_2Zn_5SnSe_8$ and $Cu_2Zn_6SnSe_9$ probably decompose into $Cu_2ZnSnSe_4 + ZnSe$.

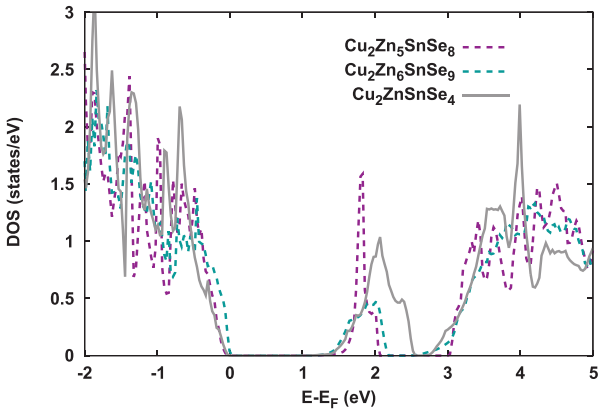

FIG. 3. Calculated DOS of $Cu_2Zn_5SnSe_8$ (purple), $Cu_2Zn_6SnSe_9$ (dark cyan), and kesterite structured $Cu_2ZnSnSe_4$ (grey), obtained from the HSE06 Kohn-Sham band structures. E_F is the Fermi energy.

According to the phase diagram reported in Refs. 8 and 9, several secondary phases exist in the pseudo-ternary $Cu_2S(e)$-ZnS(e)-$SnS(e)_2$ system. The most likely secondary phases are ZnS(e), $Cu_2S(e)$, $SnS(e)_2$, and $Cu_2SnS(e)_3$. Besides these phases, several other binary phases exist in the Cu-S(e) (e.g., CuS(e) and $Cu_{2-x}S(e)$)[39,40] and the Sn-S(e) system (e.g., SnS(e) and $Sn_2S(e)_3$).[41,42] In the Zn-S(e) system, one can find only ZnS(e) as a stable compound.[43] So far, ternary phases have been mainly studied in the Cu-Sn-S(e) system, most of them along the $Cu_2S(e)$-$SnS(e)_2$ tie line.[44,45] Little is known about chalcopyrite type compounds (e.g., $Cu_{1-x}Zn_{1-y}S(e)_{2-\delta}$) in the Cu-Zn-S(e) system or the $Zn_2Sn_xS(e)_{2x+2}$ (x = 1,2,4) chalcogels in the Zn-Sn-S(e) system.[46–48] According to Olekseyuk *et al.*, $Cu_2ZnSn_3S_8$ exists as another quaternary phase on the CZTS-SnS_2 tie line.[9] The quaternary phases $Cu_2Zn_6SnSe_9$ and $Cu_2Zn_6SnSe_9$ found in this work lie on the CZTSe-ZnSe tie line. Among all these secondary phases, $Cu_2SnS(e)_3$ (reduction of the open-circuit voltage) and $Cu_xS(e)$ (decrease of the shunt resistance) are reported to be the most detrimental phases for cell performance.[1,4,22]

As $Cu_2Zn_5SnSe_8$ and $Cu_2Zn_6SnSe_9$ may be passed from the precursor to the final absorber or may be formed during low-temperature co-evaporation of CZTSe absorber films, the question arises how these two phases affect cell performance. A first hint can be derived by considering their band gaps, even if the valence and conduction band offsets are not known. Since the calculated band gap of 1.1 eV for both $Cu_2Zn_5SnSe_8$ and $Cu_2Zn_6SnSe_9$ is higher than that of CZTSe, there will be no reduction of the open-circuit voltage. Thus, $Cu_2Zn_5SnSe_8$ and $Cu_2Zn_6SnSe_9$ are expected to be rather benign. Nevertheless, according to the band

TABLE II. Calculated energy differences per atom of different compounds with respect to the decomposition into binaries (CuSe, ZnSe, and SnSe) and into $Cu_2ZnSnSe_4 + ZnSe$. Reprinted with permission from T. Schwarz, "On the nano-scale characterization of kesterite thin-films." Ph.D. dissertation (RWTH Aachen, 2015).[50]

Compound	Binaries (meV)	$Cu_2ZnSnSe_4 + ZnSe$ (meV)
$Cu_2ZnSnSe_4$	−61	
$Cu_2Zn_2SnSe_5$	−31	+18
$Cu_2Zn_3SnSe_6$	−25	+16
$Cu_2Zn_4SnSe_7$	+3	+38
$Cu_2Zn_5SnSe_8$	−20	+10
$Cu_2Zn_6SnSe_9$	−14	+13
$Cu_2Zn_7SnSe_{10}$	+4	+29

alignment of both compounds with CZTSe and considering same doping levels, $Cu_2Zn_5SnSe_8$ and $Cu_2Zn_6SnSe_9$ will act as barriers for holes increasing the series resistance. Furthermore, the interface between these compounds and the kesterite matrix can contribute to the recombination activity increasing the reverse saturation current and reducing the open-circuit voltage. Since different doping levels in the various compounds are likely, their presence will lead to band bending and further barriers. Moreover, since $Cu_2Zn_5SnSe_8$ and $Cu_2Zn_6SnSe_9$ are small precipitates, they can reduce the grain boundary velocity by the Zener drag effect[49] and can impede the growth of CZTSe grains during the annealing step.

It should be mentioned that we cannot experimentally confirm or exclude the existence of other quaternary phases lying on the CZTSe-ZnSe tie line. Identifying phases in the $Cu_2S(e)$-$ZnS(e)$-$SnS(e)_2$ system is often hampered by the structural similarity of occurring (secondary) phases and the iso-electronic structure of Cu^+ and Zn^{2+}.

Using APT, we have found two phases of $Cu_2Zn_5SnSe_8$ and $Cu_2Zn_6SnSe_9$ composition in co-evaporated CZTSe films. DFT calculations predict that both phases exist and have a distorted zinc-blende structure. We conclude that both phases are metastable, as the energy differences with respect to the decomposition into $Cu_2ZnSnSe_4$ and ZnSe (see Table II) are positive, as calculated by DFT. The calculated band gap is 1.1 eV for both $Cu_2Zn_5SnSe_8$ and $Cu_2Zn_6SnSe_9$. Due to their larger band gap compared with CZTSe, we expect that $Cu_2Zn_5SnSe_8$ and $Cu_2Zn_6SnSe_9$ are rather benign to cell performance.

The authors thank Matthias Wuttig from RWTH Aachen as well as Susann Schorr and Galina Gurieva from Helmholtz-Zentrum Berlin for fruitful discussions. This work was funded by the German Research Foundation (DFG) (Contract No. CH 943/2-1) and by the Luxembourgish Fonds National de la Recherche. Financial support provided by French ANR (ANR-12-BS04-0001-02) was gratefully acknowledged. Computational resources were provided by French GENCI (Project No. x2013096017).

[1]S. Siebentritt and S. Schorr, Prog. Photovoltaics **20**, 512–519 (2012).
[2]W. Wang, M. T. Winkler, O. Gunawan, T. Gokmen, T. K. Todorov, Y. Zhu, and D. B. Mitzi, Adv. Energy Mater. **4**, 1301465 (2014).
[3]G. Brammertz, M. Buffière, S. Oueslati, H. ElAnzeery, K. Ben Messaoud, S. Sahayaraj, C. Köble, M. Meuris, and J. Poortmans, Appl. Phys. Lett. **103**, 163904 (2013).
[4]S. Siebentritt, Thin Solid Films **535**, 1–4 (2013).
[5]P. Jackson, D. Hariskos, R. Wuerz, O. Kiowski, A. Bauer., T. M. Friedlmeier, and M. Powalla, Phys. Status Solidi (RRL) **9**, 28–31 (2015).
[6]A. Walsh, S. Chen, S. Wei, and X. Gong, Adv. Energy Mater. **2**, 400–409 (2012).
[7]T. Maeda, S. Nakamura, and T. Wada, Thin Solid Films **519**, 7513 (2011).
[8]I. V. Dudchak and L. V. Piskach, J. Alloys Compd. **351**, 145–150 (2003).
[9]I. D. Olekseyuk, I. V. Dudchack, and L. V. Piskach, J. Alloys Compd. **368**, 135–143 (2004).
[10]A. Redinger and S. Siebentritt, Appl. Phys. Lett. **97**, 092111 (2010).
[11]A. Redinger, D. M. Berg, P. J. Dale, and S. Siebentritt, J. Am. Chem. Soc. **133**, 3320 (2011).
[12]J. J. Scragg, P. J. Dale, D. Colombara, and L. M. Peter, ChemPhysChem **13**, 3035–3046 (2012).
[13]J. J. Scragg, T. Ericson, T. Kubart, M. Edoff, and C. Platzer-Bjorkman, Chem. Mater. **23**, 4625–4633 (2011).
[14]J. T. Wätjen, J. Engman, M. Edoff, and C. Platzer-Bjorkman, Appl. Phys. Lett. **100**, 173510 (2012).
[15]C. Platzer-Björkman, J. Scragg, H. Flammersberger, T. Kubart, and M. Edoff, Sol. Energy Mater. Sol. Cells **98**, 110–117 (2012).
[16]A. Redinger, K. Hönes, X. Fontané, V. Izquierdo-Roca, E. Saucedo, N. Valle, A. Pérez-Rodríguez, and S. Siebentritt, Appl. Phys. Lett. **98**, 101907 (2011).
[17]T. Schwarz, O. Cojocaru-Mirédin, P. Choi, M. Mousel, A. Redinger, S. Siebentritt, and D. Raabe, Appl. Phys. Lett. **102**, 042101 (2013).
[18]R. A. Wibowo, W. S. Kim, E. S. Lee, B. Munir, and K. H. Kim, J. Phys. Chem. Solids **68**, 1908–1913 (2007).
[19]G. Suresh Babu, Y. B. Kishore Kumar, P. Uday Bhaskar, and S. Raja Vanjari, Sol. Energy Mater. Sol. Cells **94**, 221–226 (2010).
[20]A. J. Cheng, M. Manno, A. Khare, C. Leighton, S. A. Campbell, and E. S. Aydil, J. Vac. Sci. Technol., A **29**, 051203 (2011).
[21]M. Mousel, A. Redinger, R. Djemour, M. Arasimowicz, N. Valle, P. Dale, and S. Siebentritt, Thin Solid Films **535**, 83–87 (2013).
[22]M. Mousel, T. Schwarz, R. Djemour, T. P. Weiss, J. Sendler, J. C. Malaquias, A. Redinger, O. Cojocaru-Mirédin, P. Choi, and S. Siebentritt, Adv. Energy Mater. **4**, 1300543 (2014).
[23]T. Kelly and M. K. Miller, Rev. Sci. Instrum. **78**, 031101 (2007).
[24]A. Stein, S. W. Keller, and T. E. Mallouk, Science **259**, 1558–1564 (1993).
[25]W. E. Buhro, K. M. Hickman, and T. J. Trentler, Adv. Mater. **8**, 685–688 (1996).
[26]D. M. Berg, M. Arasimowicz, R. Djemour, L. Gütay, S. Siebentritt, S. Schorr, X. Fontané, V. Izquierdo-Roca, A. Pérez-Rodriguez, and P. Dale, Thin Solid Films **569**, 113–123 (2014).
[27]G. Kresse and J. Furthmüller, Comput. Mater. Sci. **6**, 15 (1996).
[28]G. Kresse and J. Furthmüller Phys. Rev. B **54**, 11169 (1996).
[29]S. Goedecker, J. Chem. Phys. **120**, 9911 (2004).
[30]M. Amsler and S. Goedecker, J. Chem. Phys. **133**, 224104 (2010).
[31]V. I. Anisimov, J. Zaanem, and O. K. Andersen, Phys. Rev. B **44**, 943 (1991).
[32]See supplementary material at http://dx.doi.org/10.1063/1.4934847 for the crystallographic information files.
[33]J. Heyd, G. E. Scuseria, and M. Ernzerhof, J. Chem. Phys. **118**, 8207 (2003); **124**, 219906(E) (2006).
[34]S. Botti, D. Kammerlander, and M. A. L. Marques, Appl. Phys. Lett. **98**, 241915 (2011).
[35]E. Monroy, F. Omnès, and F. Calle, Semicond. Sci. Technol. **18**, R33–R51 (2003).
[36]S. Chen, X. G. Gong, A. Walsh, and S. Wei, Appl. Phys. Lett. **94**, 041903 (2009).
[37]A. Schleife, F. Fuchs, C. Rödl, J. Furthmüller, and F. Bechstedt, Appl. Phys. Lett. **94**, 012104 (2009).
[38]L. Gütay, A. Redinger, R. Djemour, and S. Siebentritt, Appl. Phys. Lett. **100**, 102113 (2012).
[39]D. J. Chakrabarti and D. E. Laughlin, Bull. Alloy Phase Diagrams **4**, 254–258 (1983).
[40]V. M. Glazov, A. S. Pashinkin, and V. A. Fedorov, Inorg. Mater. **36**, 641–652 (2000).
[41]B. Predel and O. Madelung, "Se-Sn (selenium-tin)," in *The Landolt-Börnstein Database* (Springer-Materials, 1998).
[42]B. Predel and O. Madelung, "S-Sn (sulfur-tin)," in *The Landolt-Börnstein Database* (Springer-Materials, 1998).
[43]R. C. Sharma and Y. A. Chang, J. Phase Equilib. **17**, 155–160 (1996); **17**, 261–266 (1996).
[44]L. V. Piskach, O. V. Parasyuk, and I. D. Olekseyuk, J. Alloys Compd. **279**, 142 (1998).
[45]S. Fiechter, M. Martinez, G. Schmidt, W. Henrion, and Y. Tomm, J. Phys. Chem. Solids **64**, 1859–1862 (2003).
[46]D. P. Joseph, S. Ganesan, M. Kovendhan, S. A. Suthanthiraraj, P. Maruthamuthu, and C. Venkateswaran, Phys. Status Solidi A **208**, 2215–2219 (2011).
[47]J. R. Craig and G. Kullerud, Miner. Deposita **8**, 81–91 (1973).
[48]Y. Oh, S. Bag, C. D. Malliakas, and M. G. Kanatzidis, Chem. Mater. **23**, 2447–2456 (2011).
[49]G. Gottstein, *Materialwissenschaft der Werkstofftechnik—Physikalische Grundlagen*, 4th ed. (Springer Vieweg, Berlin, 2014), Chap. 7.
[50]T. Schwarz, "On the nano-scale characterization of kesterite thin-films," Ph.D. dissertation (RWTH Aachen, 2015).